Applied Physics A (2019) 125:15
https://doi.org/10.1007/s00339-018-2310-1

Applied Physics A
Materials Science & Processing

RAPID COMMUNICATION

A broadband plasmonic light absorber based on a tungsten meander-ring-resonator in visible region

Can Cao[1] · Yongzhi Cheng[2]

Received: 3 September 2018 / Accepted: 5 December 2018 / Published online: 10 December 2018

Abstract
We present the design and numerical simulations of a broadband plasmonic light absorber (PLA) based on a tungsten meander-ring-resonator (MRR) structure in visible region. The proposed PLA is composed of a periodic MRR array and a continuous tungsten (W) film separated by a dielectric substrate. Simulation results indicate that the absorbance of our PLA is up to 99.9% at 538 THz, and it is over 90% from 370 to 854 THz across the whole visible region. The simulated electric field distributions reveal that the stronger broadband absorption is caused by the excitation of localized surface plasmon (LSP), propagating surface plasmon (PSP) and guide mode resonances. Further simulation indicates that designed PLA is polarization insensitive and has a wide angle for both transverse electric (TE) and transverse magnetic (TM) modes. In addition, the impact of the geometric parameters of the designed PLA on the absorption spectrum was also studied systematically. Owing to its superior performance, the proposed PLA based on tungsten MRR can be a potential application in thermal imaging, emissivity control and solar energy harvesting.

1 Introduction

Plasmonic light absorber (PLA) as an important branch of optical devices is vital for its unique ability to trap light beyond diffraction limit and has potential applications in photodetections and thermal emission [1–4], thermal imaging [5], solar energy harvesting [6, 7], and sensing [8]. In past few years, PLAs based on various plasmonic nanostructures/nanoparticles and metamaterials (MMs) have been proposed and studied extensively, which could achieve strong absorption for the incident light in infrared and visible regions [9–19]. Various types of electromagnetic (EM) resonances, such as surface plasmon polaritons (SPPs), propagating surface plasmon (PSP), localized surface plasmon (LSP), and magnetic polaritons (MPs) in these PLAs are generally employed to enhance the absorption of incident light [12–19]. Desired resonance absorption features with great flexibility could be achieved by engineering the shape, size, thickness and periodicity of metallic and dielectric nanostructures of these PLAs. The perfect absorption is usually a single or multiple narrow bands due to their nature of the resonances [8, 20, 21]. However, for applications in the areas of energy harvesting and thermal emission/imaging, the broadband absorption is highly desirable.

Recent years, significant progress has been made in achieving broadband absorption with multilayered continuous metal–dielectric–metal (MDM) nanostructures in one unit-cell with overlapping resonance frequencies and this is an effective method [7, 17, 22–29]. Cui et al. proposed a broadband PLA based on multilayered sawtooth anisotropic MMs, which can realize a near perfect absorption in wavelength range of 3–5.5 μm for normal incident TM polarization light [22]. Then, Zhou et al. [23] and He et al. [24] proposed PLAs based on multilayered hyperbolic MMs, which can also realize strong broadband absorption. However, the above-mentioned PLAs suffer from a common disadvantage of being sensitive to the polarization state of incident light, thus limiting their potential applications. To overcome this disadvantage, Liang et al. [7] designed a PLA with polarization insensitive based on multi-layered pyramidal-shaped MMs, which can achieve excellent absorption of nearly 100% at full infrared waveband from 1

✉ Yongzhi Cheng
chengyz@wust.edu.cn

Can Cao
caocan@csu.edu.cn

[1] School of Physics and Electronics, Central South University, Changsha 410083, People's Republic of China

[2] School of Information Science and Engineering, Wuhan University of Science and Technology, Wuhan 430081, People's Republic of China

to 14 μm. After then, PLAs based on various multilayered nanostructures have been proposed and investigated intensively, which could achieve stronger broadband absorption with polarization insensitive [17, 25–29]. The broadband absorption window of the PLAs can be improved further by increasing the number of metal/dielectric layers. However, the broadband PLAs proposed above are rather difficult to realize experimentally since they require precise control in complex fabrication processes, which also limit their potential applications. More recently, other novel design strategies just using tri-layered nanostructure based on high index of dielectric or special metal material have been proposed [30–37], which could achieve perfect broadband absorption. These methods above show advances to ideal PLAs with high efficient broadband absorption as well as compact profile. However, these elaborate nanostructures of PLAs also could bring about fabrication difficulties and involve the time consuming and high fabrication cost. Moreover, the noble metals such as Au and Ag were used as the plasmonic materials for the previous PLAs. These conventional PLAs formed by the common noble metals are usually very weak thermal stability [38]. To Design an effective PLA with a relative simple plasmonic nanostructure to achieve broadband, polarization-independent, wide-angle and near perfect absorption is still a meaningful but challenging work, especially for visible PLA. To the best of our knowledge, there are very few tri-layered broadband, thermal stability, polarization-insensitive and wide incident angle toleration PLAs reported previously.

In this work, we present a simple design of PLA based on tri-layered MDM nanostructure that can enable high efficient absorption, broadband operation, polarization independence and wide angle in visible region. Here, we choose the tungsten to replace the common noble metals in the MDM nanostructure using its intrinsic plasmonic resonance features. The proposed PLA can be fabricated by combing the advanced electron beam lithography (EBL) and magnetron sputtering technologies [31]. The proposed PLA not only has a simple geometry and parameter adjustability-based material composition, but also shows a high absorption performance and temperature resistance. Thus, our design could be as a candidate for potential applications in thermal imaging, emissivity control and solar energy harvesting.

2 Structure design and simulation

Similarly to the previous typical design, our PLA is also formed by tri-layered MDM nanostructure with a period smaller than the operation wavelengths. For this typical MDM-based PLA, the design of resonator pattern of the front layer is vital to achieve strong broadband absorption. Generally, the modes and intensity of resonance are determined by the resonator pattern and types, and the thickness of the middle dielectric layer. By reasonable parameter design of the nanostructure, multiple resonance modes could be excited effectively for the normal incident light, thus resulting in a multi-band or strong broadband absorption [12, 36–44]. The meander wire structure has been proposed and investigated, which could support the more resonance modes for the incident light compared with counterpart wire or ring structure. Thus, the meander wire structure could be used to construct the novel and high-performance optical devices [45–47]. Based on our previous researches [44, 47], it also inspires us to use the meander wire structure to design a novel broadband PLA in visible region.

Figure 1a shows two-dimensional (2D) nanostructure array of the proposed PLA, which is composed of a metallic meander-ring-resonator (MRR) array over a continuous metallic film layer separated by a dielectric substrate. Figure 1b–d depicts the front, lattice and perspective views of the unit-cell nanostructure for the proposed PLA. It should be noticed that metallic MRR structure is derived from the square-ring-resonator (SRR) structure. It can be expected that MRR structure can support the more resonance modes for the incident light compared with counterpart SRR structure, thus resulting in a continuous strong broadband absorption. The optimized geometric parameters of the designed nanostructure are as follows: $p_x = p_y = 400$ nm, $l = 380$ nm, $w = 75$ nm, $w_0 = 15$ nm, $g = 15$ nm, $t_s = 35$ nm, $t_m = 60$ nm, $t_g = 150$ nm.

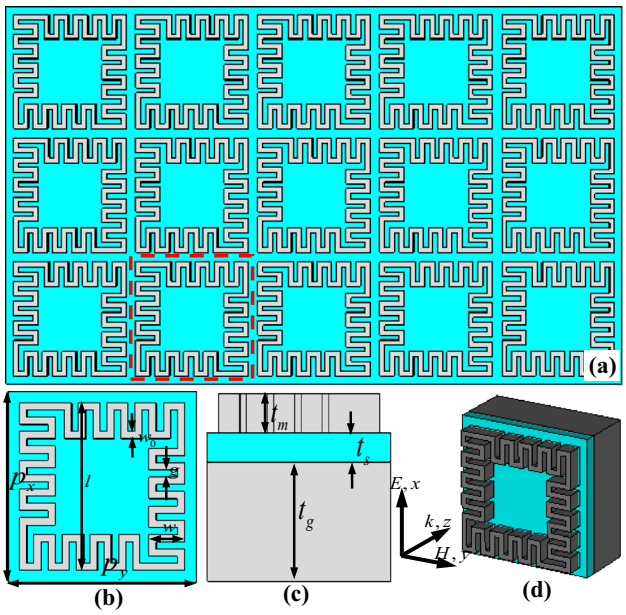

Fig. 1 Schematic illustration of the proposed PLA: **a** two-dimensional (2D) nanostructure array, **b–d** front, lattice and perspective views of the unit-cell nanostructure

To investigate its efficiency of the proposed PLA, we performed a full wave simulation using the frequency domain solver based on the finite integration technique (FIT) in CST Microwave Studio. In simulation, the front and back metallic layers are selected as tungsten film, which is described as the dielectric in visible region detailed in Ref [48]. Tungsten, also known as wolfram (W), has remarkable robustness for the fact that it has the highest melting point (3410 °C), which has been used to design PLAs in near-infrared region [39–41]. Tungsten is an impressive refractory material with high melting points, which has been widely used in aeronautics and astronautics fields. The thickness of back continuous tungsten film is 150 nm, which is much larger than the typical skin depth in visible regime (to avoid transmission through the gold film), while the 35-nm-thick high-melting-point SiO_2 film was selected as a middle dielectric substrate, which is an optically transparent and lossless dielectric with permittivity of 2.1 and a melting point of 1600 °C [12]. In simulation process, the periodic boundary conditions are applied along the *x*- and *y*-axis directions for the transverse boundaries to replicate an infinite array of the PLA, and the perfectly matched layers are applied along the *z*-axis direction [44]. As shown in Fig. 1d, the periodic nanostructure array is illuminated by a normally incident light with the electric field parallel to the *x*-axis and the magnetic field parallel to the *y*-axis direction, respectively. Since the incident light is blocked off by the back continuous gold film, just the reflection need to be considered, the absorbance can be calculated by $A(\omega)=1-R(\omega)$, where $R(\omega)$ is the reflectance as functions of frequency ω.

3 Results and discussion

Figure 2a presents the simulated reflectance and absorbance spectra of the proposed PLA for the normal incident light in visible regime. It can be observed that the reflectance is below 10%, and the corresponding absorbance is greater than 90% from 370 to 854 THz, completely across the entire visible region. Thus, the relative bandwidth of the absorbance over 90% is about 79.1%. In addition, the absorbance is over 99% from 483 to 605 THz, which is a nearly complete absorption for the incident light. For comparison, we also give the absorbance spectrum of the PLA based on the SRR structure, as shown in Fig. 1b. The size of the SRR is the same with the MRR structure in simulation. It can be seen that the absorbance of the SRR-based PLA is over 90% in some resonance frequencies. However, the continuous strong absorption (over 90%) in a broadband frequency range in the same visible frequency range cannot be achieved. Obviously, the continuous broadband absorption performance of the proposed PLA based on MRR is more superior compared with the SRR. Thus, this design can be an expected application in the solar energy harvesting due to its broadband and stronger absorption properties.

To reveal the physical mechanism behind the stronger broadband absorption of the proposed PLA, we studied the distributions of electric (E_x, *y*–*z* plane) and magnetic (H_y, *x*–*z* plane) fields of the middle plane of the unit-cell structure at different resonance frequencies ($f_1=400$ THz, $f_2=538$ THz, and $f_3=700$ THz). As shown in Fig. 3a–c, one can be seen that the localized electric fields are enhanced and concentrated on both side (right and left sides) edges and corners of MRR and the middle dielectric layer of the proposed PLA nanostructure. As shown in Fig. 3d–f, strong magnetic fields are mainly confined in the dielectric layer between the top metal MRR and the bottom metal film. Essentially, surface plasmon polariton (SPPs) modes are excited in the nanostructure where the incident light is coupled into the air-slit and localized around the metal edges and corners between neighboring unit-cells, creating SPP-induced light absorption at above frequencies [12, 37, 49]. The SPPs are usually formed by the interaction between external incident light and free electrons in the nanostructure along the wave propagation direction [17, 31]. This means that the SPPs have remarkable field enhancement effect to increase the absorption level of the proposed PLA [37]. However, the distributions of the EM field are intrinsically different at

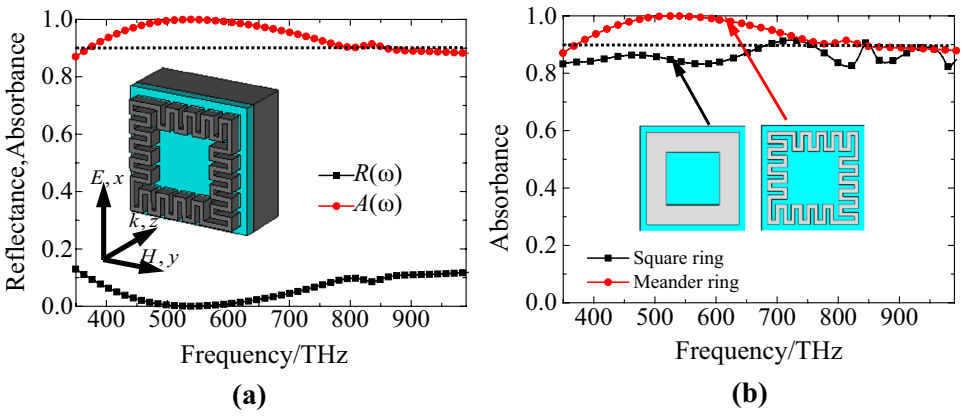

Fig. 2 The simulated **a** reflectance ($R(\omega)$) and absorbance ($A(\omega)$) of the designed PLA based on MMR, **b** the comparison of the absorbance of the PLAs based on SRR and MMR

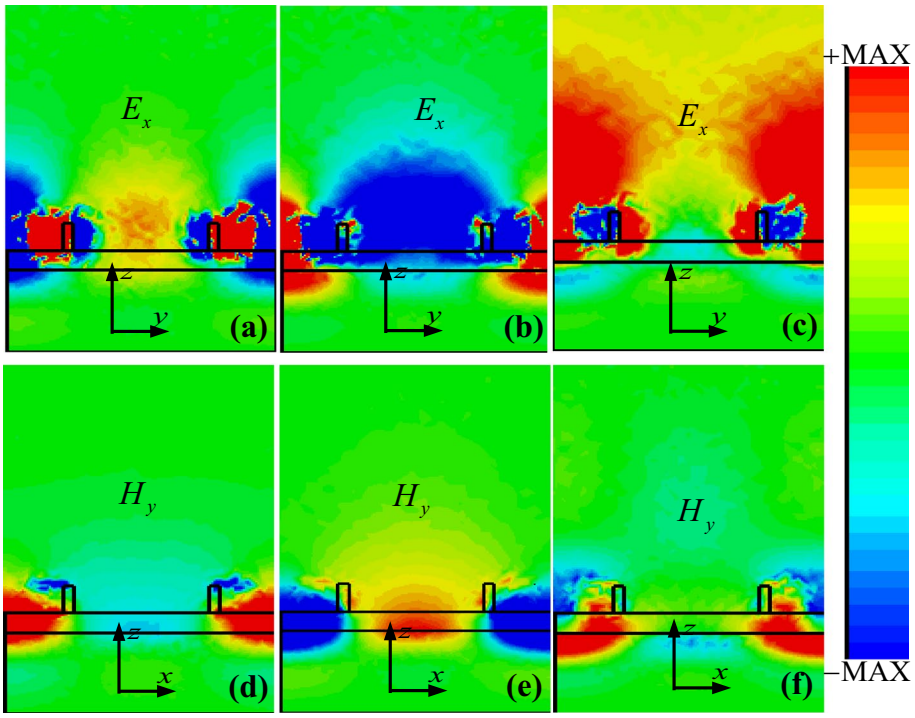

Fig. 3 Distributions of the electric field E_x (in the y–z plane of $x=0$) and the magnetic field H_y (in the x–z plane of $y=0$) of the middle plane of the unit-cell structure at different resonance frequencies: **a, d** $f_1=400$ THz; **b, e** $f_2=538$ THz, and **c, f** $f_3=700$ THz

different resonance frequencies. The incident light energy loss induced by the excitation of SPPs mode in the designed nanostructure is large enough to enhance absorption at resonances [16, 50, 51]. At the first frequency of $f_1=400$ THz, as shown in Fig. 3a, d, the electric and magnetic fields are mainly located in the middle SiO_2 layer and also enhanced intensively between the adjacent unit-cells, revealing that the perfect absorption originates from the excitation of the localized surface plasmon (LSP) mode [17, 37]. At the second and third frequencies of $f_2=538$ THz and $f_3=700$ THz, from Fig. 3e, f, the magnetic field is not only located in the SiO_2 layer and enhanced between the adjacent cells but also localized on the interfaces of W/SiO_2 and SiO_2/W, indicating that the perfect absorption mainly stems from the hybridization effect of the LSP mode, propagating surface plasmon (PSP) mode and guide mode [37, 38]. Thus, the combined contribution of SPP resonance with different modes and guide modes together leads to a strong broadband absorption in visible regime.

To further get insight on the physical mechanism of the proposed PLA for normal incident lights, we also study the energy flux distributions (power flow streams in x–z plane) at different resonance frequencies ($f_1=400$ THz, $f_2=538$ THz, and $f_3=700$ THz), as shown in Fig. 4. It can be observed that the input energy fluxes are originally parallel streams in the space far away from the nanostructure at above resonance frequencies. When the light streams move closer to and across the nanostructure, the most energy of the power flow becomes curled and finally concentrate on the vicinity of the edges, slits and corners of the nanostructure. It is evident

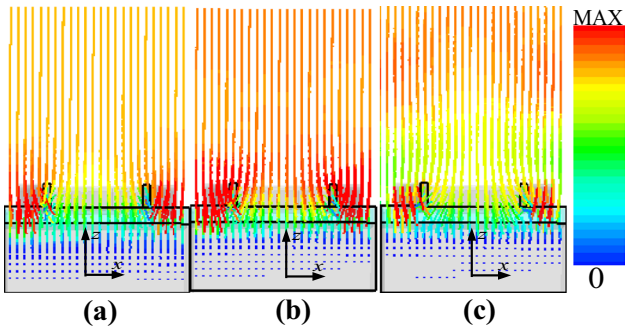

Fig. 4 The distributions of the power flow streams in x–z plane at different resonance frequencies: **a** $f_1=400$ THz, **b** $f_2=538$ THz, and **c** $f_3=700$ THz

that the energy flux can gather on the surfaces of the MRR structure, and it decays with the transmission of lights. It means that the incident light energy flows from the top part to the bottom of the nanostructure, and the residual one goes into the continuous tungsten film and finally decay completely. From Fig. 4a–c, at different resonance frequency, the energy flux distributions in nanostructure are also different due to the excitations of different resonance modes for the incident light.

For practical application, the broadband absorption properties of the proposed PLA should be robust for different polarization and incident angles for both TE and TM modes. Thus, it needs to exam the polarization and incidence angle dependence of the designed PLA for both TE and TM waves, as shown in Fig. 5. From Fig. 5a, b, it can

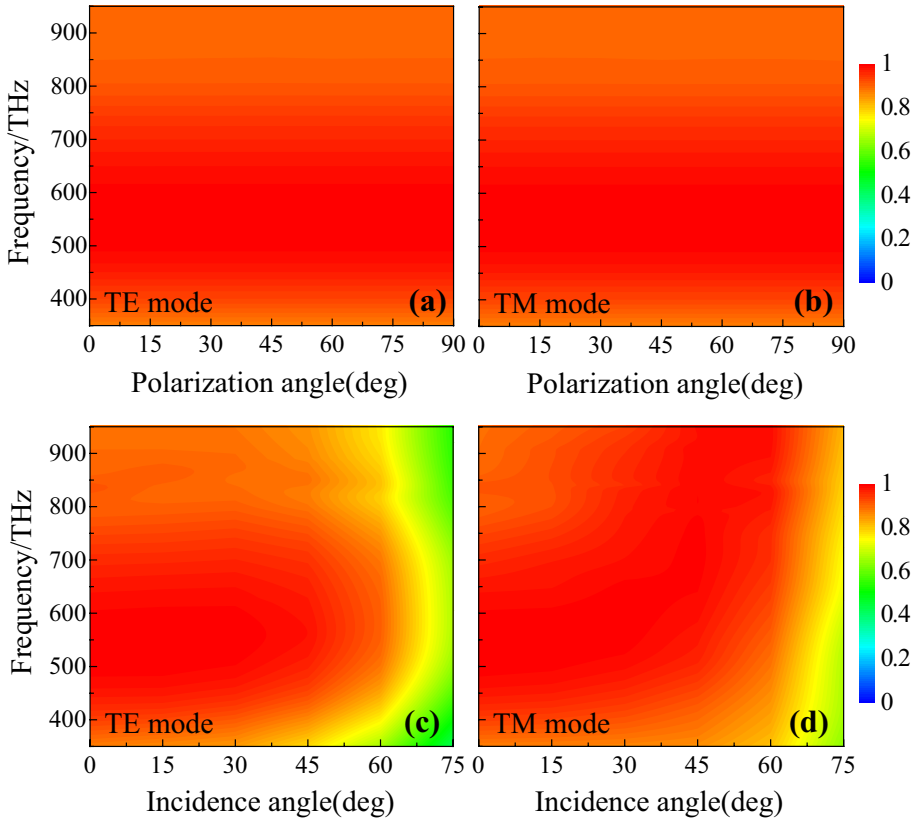

Fig. 5 Simulated absorbance as a function of **a, b** polarization angles and **c, d** incident angles with different polarization modes: **a, c** TE mode; **b, d** TM mode

be observed clearly that the absorbance is unchanged completely with different polarization angles for both the TE and TM modes due to the high rotational symmetry of the unit-cell nanostructure.

For the oblique incidence, as shown in Fig. 5c, d, we can see that the proposed PLA can keep a high performance over a wide range of incidence angles for both TE and TM modes. However, when the incident angle increases to a certain value, the performance will be deteriorated gradually. From Fig. 5c, for TE mode, the absorption level can remain stable over a broadband frequency range when the incident angle is below 50°. Beyond 50°, the absorbance decreases gradually at some frequency regions when increasing incident angle (> 50°). It is because the electric resonance modes cannot be excited effectively when the incident angle is greater than a certain value (> 50°) in this case. For TM mode, as shown in Fig. 5d, it can be seen that the absorbance is nearly unchanged when the incident angle is below 60°. Beyond 60°, the broadband absorption performance will be deteriorated gradually with further increasing incident angle. However, the decrease of the absorbance for TM mode is not obvious compared with the one for the TE mode, since the magnetic response plays a dominant role over the electric response for TM mode. Such broadband PLA is very desirable for potential applications in photovoltaics, thermal emitters, and solar energy harvesting since it is polarization insensitive and tolerated a wide incident angle for both TE and TM modes.

The absorption properties of the designed PLA under different structural geometric parameters of the unit-cell are also investigated numerically. We mainly consider four parameters of the nanostructure: side length (l), wire width (w) and thickness (t_m) of MRR structure, and thickness (t_s) of SiO_2 substrate. As shown in Fig. 6a–d, we present the absorbance spectra with four different parameters (l, w_0, t_m, and t_s), when changing only one parameter at a time, while keeping the other parameter values unchanged. From Fig. 6a–d, we can see that the all absorption peak frequencies are decreased gradually with the increase of the geometrical parameters (l, w_0, t_m, and t_s). As is well known, the resonance absorption mechanisms created by the PLA usually can be analyzed quantitatively by the equivalent LC resonance circuit theory [16, 39, 40]. For our proposed PLA, the equivalent capacitor (C) and inductance (L) are associated with the geometrical parameters of the unit-cell structure. The resonance absorption frequency can be expressed as $f_m = 1/2\pi\sqrt{LC}$, which is near inversely proportional to the geometrical parameters of the proposed PLA. The equivalent C or L will be increased with the increase of the geometrical parameters, thus leading to the decrease of the resonance absorption frequency. In addition, a much broader strong absorption (> 90%) spectrum can be obtained for the

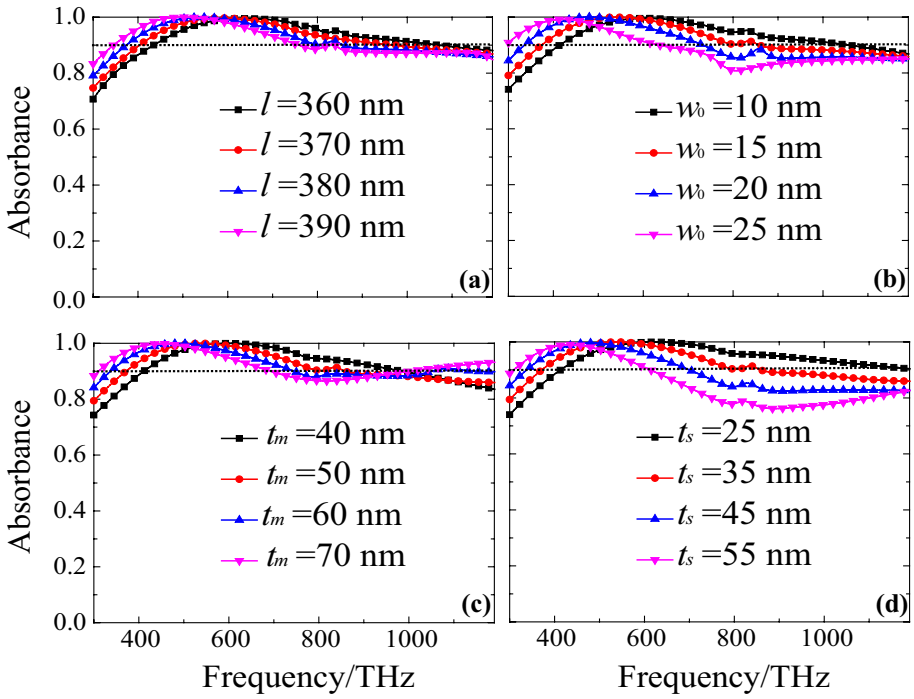

Fig. 6 Simulated absorbance spectra for different geometric parameters: **a**–**c** side length (l), wire width (w_0) and thickness (t_m) of the MRR structure; **d** thickness (t_s) of SiO_2 substrate

PLA nanostructure with a smaller geometrical parameter. For example, as shown in Fig. 6d, when $t_s = 25$ nm, the relative bandwidth of the absorbance of over 90% is up to the maximal value of about 97.4%. Thus, we can conclude that the resonance absorption properties of the proposed PLA can be adjusted dynamically by changing the geometrical parameters of the unit-cell structure.

4 Conclusions

In conclusion, a broadband PLA based on tungsten MRR structure in visible region is proposed and investigated numerically. The absorbance of over 90% on average in a frequency range from 370 to 854 THz under normal incidence can be obtained. The simulation results indicate that the proposed PLA is polarization independent for normal incident light, and broadband absorption performance is also excellent over a wide incident angle range for both TE and TM modes, which is beneficial for practical application. The distributions of the electric and magnetic in the nanostructure field reveal that the stronger broadband absorption performance is mainly attributed to combination excitations of multiple resonances of LSPs, PSPs and guide modes. Thus, the EM fields of the incident light are enhanced extremely and contributed to the strong absorption of the proposed PLA in a broadband frequency range. Further simulation results indicate that the absorption properties can be adjusted dynamically by varying the geometrical parameters of the unit-cell structure. Additionally, the tungsten and SiO_2 are both high-melting-point and refractory materials, which suggest an excellent stability under high-temperature and high-power surroundings of the proposed PLA. Due to the attractive and favorable properties, the proposed PLA can make it as an attractive candidate for the widely promising applications in thermal emitters, solar photovoltaic, and solar energy harvesting.

Acknowledgements This work was supported by the National Natural Science Foundation of China (Grant nos. 61504171, 61605147), the Natural Science Foundation of Hubei China (Grant no. 2017CFB588), and the Science and Technology Research Project of Education Department of Hubei China (Grant no. D20181107).

References

1. T. Maier, H. Brückl, Wavelength-tunable microbolometers with metamaterial absorbers. Opt. Lett. **34**(19), 3012–3014 (2009)
2. F.B.P. Niesler, J.K. Gansel, S. Fischbach, M. Wegener, Metamaterial metal-based bolometers. Appl. Phys. Lett. **100**(20), 203508 (2012)
3. Y. Qu, Q. L i, K. D u, L. Ca i, J. Lu, M. Qiu, Dynamic thermal emission control based on ultrathin plasmonic metamaterials including phase-changing material GST. Laser Photonics Rev. **11**(5), 1700091 (2017)
4. Y. Qu, Q. Li, L. Cai, M. Pan, P. Ghosh, K. Du, M. Qiu, Thermal camouflage based on the phase changing material GST. Light Sci. Appl. **7**, 26 (2018)
5. N. Landy, C.M. Bingham, T. Tyler, N. Jokerst, D.R. Smith, W.J. Padilla, Design, theory, and measurement of a polarization-insensitive absorber for terahertz imaging. Phys. Rev. B **79**, 125104 (2009)

6. H.A. Atwater, A. Polman, Plasmonics for improved photovoltaic devices. Nat. Mater. **9**, 205 (2010)
7. Q. Liang, T. Wang, Z. Lu, Q. Sun, Y. Fu, W. Yu, Metamaterial-based two dimensional plasmonic subwavelength structures offer the broadest waveband light harvesting. Adv. Opt. Mater. **1**, 43–49 (2013)
8. Y. Cheng, X.S. Mao, C. Wu, L. Wu, R.Z. Gong, Infrared non-planar plasmonic perfect absorber for enhanced sensitive refractive index sensing. Opt. Mater. **53**, 195–200 (2016)
9. J. Hao, J. Wang, X.L. Liu, W.J. Padilla, L. Zhou, M. Qiu, High performance optical absorber based on a plasmonic metamaterial. Appl. Phys. Lett. **96**, 251103–251104 (2010)
10. X. Chen, B. Jia, J.K. Saha, B. Cai, N. Stokes, Q. Qiao, Y. Wang, Z. Shi, M. Gu, Broadband enhancement in thin-fim amorphous silicon solar cells enabled by nucleated silver nanoparticles. Nano Lett. **12**, 2187–2192 (2012)
11. S. Butun, K. Aydin, Structurally tunable resonant absorption bands in ultrathin broadband plasmonic absorbers. Opt. Express **22**, 19457–19468 (2014)
12. W. Li, U. Guler, N. Kinsey, G.V. Naik, A. Boltasseva, J. Guan, V.M. Shalaev, A.V. Kildishev, Refractory plasmonics with titanium nitride: broadband metamaterial absorber. Adv. Mater. **26**, 7959–7965 (2014)
13. A. Vora, J. Gwamuri, N. Pala, A. Kulkarni, J.M. Pearce, D. Güney, Exchanging ohmic losses in metamaterial absorbers with useful optical absorption for photovoltaics. Sci. Rep. **4**(1), 4901 (2015)
14. L. Zhou, Y. Zhou, Y.F. Zhu, X.X. Dong, B.L. Gao, Y.Z. Wang, S. Shen, Broadband bidirectional visible light absorber with wide angular tolerance. J. Mater. Chem. C. **4**, 391 (2016)
15. A.K. Azad, W.J.M. Kort-Kamp, M. Sykora, N.R. Weisse-Bernstein, T.S. Luk, A.J. Taylor, D.A.R. Dalvit, H.T. Chen, Metasurface broadband solar absorber. Sci. Rep. **6**(1), 20347 (2016)
16. H. Luo, Y.Z. Cheng, Design of an ultrabroadband visible metamaterial absorber based on three-dimensional metallic nanostructures. Mod. Phys. Lett. B **31**, 1750231 (2017)
17. D. Wu, C. Liu, Y. Liu, L. Yu, Z. Yu, L. Chen, R. Ma, H. Ye, Numerical study of an ultra-broadband near perfect solar absorber in the visible and near-infrared region. Opt. Lett. **42**(3), 450–453 (2017)
18. C. Cao, Y. Cheng, Quad-band plasmonic perfect absorber for visible light with a patchwork of silicon nanorod resonators. Materials **11**(10), 1954 (2018)
19. Z. Liu, G. Liu, Z. Huang, X. Liu, G. Fu, Ultra-broadband perfect solar absorber by an ultra-thin refractory titanium nitride metasurface. Sol. Energy Mater. Sol. Cell. **179**, 346–352 (2018)
20. J. Xu, Z. Zhao, H. Yu, L. Yang, P. Gou, J. Cao, Y. Zou, J. Qian, T. Shi, Q. Ren, Z. An, Design of triple-band metamaterial absorbers with refractive index sensitivity at infrared frequencies. Opt. Express **24**(22), 25742–25751 (2016)
21. Y. Cheng, H. Zhang, X.S. Mao, R.Z. Gong, Dual-band plasmonic perfect absorber based on all-metal nanostructure for refractive index sensing application. Mater. Lett. **219**, 123–126 (2018)
22. Y.K.H. Cui, J. Fung, H. Xu, Y. Ma, S. Jin, He, N.X. Fang, Ultra-broadband light absorption by a sawtooth anisotropic metamaterial slab. Nano Lett. **12**, 1443–1447 (2012)
23. J. Zhou, A.F. Kaplan, L. Chen, L.J. Guo, Experiment and theory of the broadband absorption by a tapered hyperbolic metamaterial array. ACS Photonics **1**(7), 618–624 (2014)
24. S. He, F. Ding, L. Mo, F. Bao Light absorber with an ultra-broad flat band based on multi-sized slow-wave hyperbolic metamaterial thin-films. Progr. Electromagn. Res. **147**, 69–79 (2014)
25. H. Ko, D.H. Ko, Y. Cho, I.K. Han, Broadband light absorption using a multilayered gap surface plasmon resonator. Appl. Phys. A **116**, 857–861 (2014)
26. X. Yin, L. Chen, X. Li, Ultra-broadband super light absorber based on multi-sized tapered hyperbolic metamaterial waveguide arrays. J. Lightwave Technol. **33**(17), 3704–3710 (2015)
27. J. Wu, Polarization-independent broadband absorber based on pyramidal metal-dielectric grating structure. Opt. Mater. **62**, 47–51 (2016)
28. P. Liu, T. Lan, Wide-angle, polarization-insensitive, and broadband metamaterial absorber based on multilayered metal-dielectric structures. Appl Opt **56**(14), 4201–4205 (2017)
29. D. Wu, C. Liu, Y. Liu, Z. Xu, Z. Yu, L. Yu, L. Chen, R. Ma, J. Zhang, H. Ye, Numerical study of a wide-angle polarization independent ultra-broadband efficient selective metamaterial absorber for near-ideal solar thermal energy conversion. RSC Adv. **8**, 21054 (2018)
30. Y. Lu, W. Dong, Z. Chen, Z. Wang, S.I. Bozhevolnyi, Gap-plasmon based broadband absorbers for enhanced hot-electron and photocurrent generation. Sci. Rep. **6**, 30650 (2016)
31. D. Hu, H.Y. Wang, Q.F. Zhu, Design of an ultra-broadband and polarization-insensitive solar absorber using a circular-shaped ring resonator. J. Nanophotonics **10**(2), 026021 (2016)
32. M. Luo, S. Shen, L. Zhou, S. Wu, Y. Zhou, L. Chen, Broadband, wide-angle, and polarization-independent metamaterial absorber for the visible regime. Opt. Express **25**(14), 16715–16724 (2017)
33. M. Zhong, S.J. Liu, B.L. Xu, J. Wang, H.Q. Huang, Single-band high absorption and coupling between localized surface plasmons modes in a metamaterials absorber. Opt. Mater. **72**, 283–288 (2017)
34. W. Wang, Y. Qu, K. Du, S. Bai, J. Tian, M. Pan, H. Ye, M. Qiu, Q. Li, Broadband optical absorption based on single-sized metal-dielectric-metal plasmonic nanostructures with high- ε'' metals. Appl. Phys. Lett. **110**, 101101 (2017)
35. M. Prasanta, C.N. Rao, Period- and cavity-depth-dependent plasmonic metamaterial perfect absorber at visible frequency: design rule. J. Nanophoton. **11**(3), 036003 (2017)
36. Y. Huang, L. Liu, M. Pu, X. Li, X. Ma, X. Luo, A refractory metamaterial absorber for ultra-broadband, omnidirectional and polarization-independent absorption in the UV-NIR spectrum. Nanoscale **10**, 8298–8303 (2018)
37. L. Lei, S. Li, H. Huang, K. Tao, P. Xu, Ultra-broadband absorber from visible to near infrared using plasmonic metamaterial. Optic Express **26**, 5686–5693 (2018)
38. X. Chen, Y. Chen, M. Yan, M. Qiu, Nanosecond photothermal effects in plasmonic nanostructures. ACS Nano **6**, 2550–2557 (2012)
39. C.J. Chen, J.S. Chen, Y.B. Chen, Optical responses from lossy metallic slit arrays under the excitation of a magnetic polariton. J. Opt. Soc. Am. B **28**(8), 1798–1806 (2011)
40. Z. Li, L. Stan, A. David, X. Czaplewski, J. Yang, Gao, Wavelength-selective mid-infrared metamaterial absorbers with multiple tungsten cross resonators. Opt. Express **26**(5), 5616–5631 (2018)
41. B. Wei, S. Jian, A near-infrared perfect absorber assisted by tungsten covered ridges. Plasmonics (2018). https://doi.org/10.1007/s11468-018-0791-6
42. D. Govind, S.A. Ramakrishna, Multipolar localized resonances for multi-band metamaterial perfect absorbers. J. Opt. **16**, 094016 (2014)
43. J. Nath, S. Modak, I. Rezadad, D. Panjwani, F. Rezaie, J.W. Cleary, R.E. Peale, Far-infrared absorber based on standing-wave resonances in metal-dielectric-metal cavity. Opt. Express **23**, 20366–20380 (2015)
44. Y.Z. Cheng, M.L. Huang, H.R. Chen, Z.Z. Guo, R.Z. Gong, X.S. Mao, Ultrathin six-band polarization-insensitive perfect metamaterial absorber based on a cross-cave patch resonator for terahertz waves. Materials **10**, 591 (2017)

45. J.Y. Ou, E. Plum, J. Zhang, N.I. Zheludev, An electromechanically reconfigurable plasmonic metamaterial operating in the near-infrared. Nat. Nanotechnol **8**(4), 252–255 (2013)
46. P. Fei, Z. Shen, X. Wen, F. Nian, A single-layer circular polarizer based on hybrid meander-line and loop configuration. IEEE Trans. Antennas Propag. **63**(10), 4609–4614 (2015)
47. Y.Z. Cheng, C. Fang, X.S. Mao, R.Z. Gong, L. Wu, Design of an ultrabroadband and high-efficiency reflective linear polarization convertor at optical frequency. IEEE Photonics J. **8**(6), 1–9 (2016)
48. M.A. Ordal, L.L. Long, R.J. Bell, S.E. Bell, R.R. Bell, R.W. Alexander Jr., C.A. Ward, Optical properties of the metals Al, Co, Cu, Au, Fe, Pb, Ni, Pd, Pt, Ag, Ti, and W in the infrared and far infrared. Appl. Opt. **22**, 1099–1120 (1983)
49. A.V. Zayats, I.I. Smolyaninov, A.A. Maradudin, Nano-optics of surface plasmon polaritons. Phys. Rep. **408**(3), 131–314 (2005)
50. B. Gangadhar, S.A. Ramakrishna, Tri-layered composite plasmonic structure with a nanohole array for multiband enhanced absorption at visible to NIR frequencies: plasmonic and metamaterial resonances. J. Phys. D: Appl. Phys. **49**, 075103 (2016)
51. C. Cao, Y.Z. Cheng, Quad-band plasmonic perfect absorber for visible light with a patchwork of silicon nanorod resonators. Materials **11**(10), 1954 (2018)